Metal-Organic-Framework-Mediated Nitrogen-Doped Carbon for CO_2 Electrochemical Reduction

Wang, Riming; Sun, Xiaohui; Ould-Chikh, Samy; Osadchii, Dmitrii; Bai, Fan; Kapteijn, Freek; Gascon, Jorge

DOI
10.1021/acsami.8b02226

Publication date
2018

Published in
ACS Applied Materials and Interfaces

Metal-Organic-Framework-Mediated Nitrogen-Doped Carbon for CO2 Electrochemical Reduction

Article *in* ACS Applied Materials & Interfaces · April 2018
DOI: 10.1021/acsami.8b02226

7 authors, including:


Riming Wang
Delft University of Technology
1 PUBLICATION **0** CITATIONS
SEE PROFILE


Xiaohui Sun
Delft University of Technology
15 PUBLICATIONS **111** CITATIONS
SEE PROFILE


Samy Ould-Chikh
King Abdullah University of Science and Technology
42 PUBLICATIONS **335** CITATIONS
SEE PROFILE


Dmitrii Osadchii
Delft University of Technology
14 PUBLICATIONS **88** CITATIONS
SEE PROFILE

Energy, Environmental, and Catalysis Applications

Metal-organic Framework-mediated Nitrogen-doped Carbon for CO2 Electrochemical Reduction

Riming Wang, Xiaohui Sun, Samy Ould-Chikh, Dmitrii Osadchii, Fan Bai, Freek Kapteijn, and Jorge Gascon

ACS Appl. Mater. Interfaces, **Just Accepted Manuscript** • DOI: 10.1021/acsami.8b02226 • Publication Date (Web): 11 Apr 2018

Metal-organic Framework-mediated Nitrogen-doped Carbon for CO_2 Electrochemical Reduction

Riming Wang,‡[a] Xiaohui Sun,‡[a] Samy Ould-Chikh,[b] Dmitrii Osadchii,[a] Fan Bai,[a] Freek Kapteijn,[a] and Jorge Gascon[a,b]*

a. Catalysis Engineering, Dept. of Chemical Engineering, Faculty of Applied Sciences, Delft University of Technology, van der Maasweg 2629 HZ Delft, The Netherlands.

b. King Abdullah University of Science and Technology, KAUST Catalysis Center, Advanced Catalytic Materials, Thuwal 23955, Saudi Arabia.

ABSTRACT: A Nitrogen-doped carbon was synthesized through the pyrolysis of the well-known metal-organic framework ZIF-8, followed by a subsequent acid treatment, and has been applied as catalyst in the electrochemical reduction of carbon dioxide. The resulting electrode shows Faradaic efficiencies to carbon monoxide as high as ~78%, with hydrogen being the only by-product. Pyrolysis temperature determines the amount and the accessibility of N species in the carbon electrode, in which pyridinic-N and quaternary-N species play key roles in the selective formation of carbon monoxide.

KEYWORDS: Nitrogen-doped carbon, electrocatalyst, ZIF-8, MOF-mediated synthesis, CO_2 electrochemical reduction

1. INTRODUCTION

CO_2 concentration in the atmosphere has increased drastically since the first industrial revolution. The current CO_2 level is considered to have caused severe environmental problems,[1] increasing the need to find solutions both to revert CO_2 emissions and to utilize the CO_2 already present in the atmosphere. In both cases, valorization of CO_2 (as opposite to disposal or storage) may provide human kind with new routes for the production of important chemical commodities traditionally manufactured from oil. Several pathways have been proposed to utilize CO_2,[2] such as CO_2 methanation,[3-8] reverse water gas shift,[9-13] CO_2 hydrogenation to hydrocarbons or alcohols,[14-20] CO_2 electrochemical reduction,[21-26] and CO_2 photocatalytic reduction,[27] *etc*. Among the above-mentioned CO_2 utilization methods, the electrochemical reduction of CO_2 seems to hold great promise in a more than likely future scenario with affordable green electricity at moderate prices. In such a scenario, it is highly desirable to selectively produce one single product, while the integration of CO_2 reduction products with existing chemo-catalytic technologies would be ideal. In this sense, the selective production of carbon monoxide is regarded as one of the most promising alternatives, CO being a very valuable intermediate in chemical synthesis.

Various electrocatalysts, including noble and earth-abundant metals and their coordination complexes, have been widely studied in CO_2 electroreduction reaction.[28-29] Copper is found to be active in direct synthesis of hydrocarbons and oxygenates from CO_2.[30] Silver and gold electrodes are reported to selectively convert CO_2 to CO.[31-32] Nevertheless, their limited availability and proneness to poisoning to a large extent impede the practical applications. Hence, the exploration of alternative materials with high energy efficiency, selectivity, and durability remains challenging.

Recently, introduction of heteroatoms (*e.g.* N, S, P *etc.*) into the carbon structure has been reported to improve the chemical, electrical, and functional properties of carbon materials.[33]

For instance, a carbon nanotubes (CNTs) with N as dopant show a high efficiency in CO_2 reduction to CO, while the nitrogen-free CNTs only produce very little amount of CO. The high CO selectivity was later attributed to the presence of pyridinic-N and quaternary-N.[34-35] Zhang *et al.* also investigated the effect of N content in the N-doped CNTs on the catalytic activity in this reaction, and found an linear increase of the Faradaic efficiency toward formate with the N content.[36]

Metal-organic-frameworks (MOFs) have been shown to be excellent catalyst precursors.[37-41] The controlled thermal decomposition of MOFs in an inert atmosphere is a facile synthesis method to produce carbon materials with well-developed porosity.[42-43] In this study, a prototypical MOF, ZIF-8 with a nitrogen-rich organic linker, was chosen as a sacrificial template for the synthesis of N-doped carbon catalysts (NC-T, T referring the pyrolysis temperature). The synthesis involves high-temperature pyrolysis and a subsequent acid treatment (Scheme 1). The as-synthesized N-doped carbon samples were then used for CO_2 electrochemical reduction.

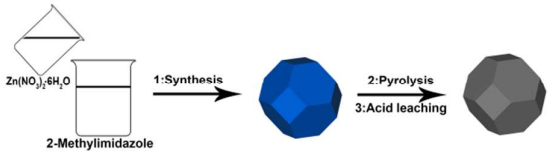

Scheme 1. Schematic illustration of the route to synthesize the NC-T catalysts. (1) Room temperature synthesis of ZIF-8 crystals. (2) Pyrolysis of the ZIF-8 crystals in N_2 at different temperatures. (3) Acid leaching to generate the NC-T catalysts.

2. EXPERIMENTAL SECTION

2.1. Materials. 2-Methylimidazole (MeIm, purity 99%), zinc nitrate hexahydrate ($Zn(NO_3)_2 \cdot 6H_2O$, >98%), zinc acetate dihydrate ($Zn(OAc)_2 \cdot 2H_2O$, >98%) and methanol

(>99.8%) were purchased from Sigma-Aldrich Chemical Co. All the chemicals were used without further purification.

2.2. Characterization techniques. X-ray diffraction (XRD) measurements were conducted on a Bruker D8 Advance X-ray diffractometer equipped with a Co-*Kα* radiation source (λ = 0.179026 nm). Raman spectra were obtained with a commercial Renishaw in Via Reflex confocal microscope using a 532 nm laser, and measurements were performed without any pre-treatment of samples at ambient conditions. Thermogravimetric (TG) analyses were collected using a Mettler Toledo TGA/SDTA851e instrument. The experiments were carried out from 25 °C to 1000 °C with a ramp of 5 °C·min^{-1} under a N_2 flow (100 mL·min^{-1}). The N_2 adsorption-desorption isotherms were measured with a Micromeritics Tristar 3020 apparatus at 77 K. Scanning electron microscopy (SEM) analysis and the EDX element mapping were performed on a Nova Nano 630 scanning electron microscope manufactured by FEI Company. Transmission electron microscopy (TEM) analysis was carried out using a FEI Titan 80-300 ST transmission electron microscope operated at 300 kV. XPS spectra were measured on a K-alpha Thermo Fisher Scientific spectrometer using monochromatic Al-*Kα* radiation at room temperature and pressure inside the analysis chamber of about 10^{-8} mbar. The obtained spectra were calibrated by setting the main peak of carbon (C*1s*) line to the reference value of Eb = 284.8 eV. Thermo Avantage software package was applied for spectra processing and analysis. The spectra were deconvoluted using a mixed Gauss-Lorentz function (20% Lorentzian contribution for C*1s*, N*1s*, and O*1s*, 30% for Zn*2p*). Scoffield sensitivity factors were used for the quantitative analysis. TPP-2M method was applied to eliminate the difference in analysis depth for different photoelectron lines.

2.3. Catalysts synthesis

2.3.1. Synthesis of ZIF-8. ZIF-8 precursors were synthesized according to a previously reported method with some modification.[44] Typically, the metal precursor and organic linker

solutions were prepared by separately dissolving 2.933 g zinc nitrate hexahydrate and 6.489 g 2-methylimidazole into 200 mL methanol and kept under stirring for 15 min. The clear linker solution was then rapidly mixed with the metal precursor solution and kept under magnetic stirring at room temperature for 24 h. Afterwards, the bright white product was collected by filtration, washed three times with methanol, and dried at 80 °C under vacuum.

2.3.2. Synthesis of MOF-5. MOF-5 precursors were synthesized based on the previously reported method with some modification.[45] In a typical synthesis, 5.065 g terephthalic acid and 16.99 g zinc acetate dihydrate were dissolved in 400 mL and 500 mL DMF, respectively. After stirring for 15 min, the zinc acetate solution was added to the organic linker solution, and the mixture was stirred for another 2.5 h. The product was filtered and washed three times with DMF. The final product was dried at 80 °C under vacuum.

2.3.3. Synthesis of NC-T and C-900. For the preparation of NC-T, 1g ZIF-8 was pyrolyzed in a ceramic crucible inside a tubular quartz reactor (approximately 1.0 m in length and 5.0 cm in diameter) horizontally placed in a ceramic fiber oven (Carbolite, Sheffield). Nitrogen was kept flushing through the reactor at a rate of 100 $ml \cdot min^{-1}$ under 30 °C for 0.5 h,, followed by further carbonization at different temperature for 4 h under the same N_2 flow. The set temperature was reached at a ramp of 2 $°C \cdot min^{-1}$. The obtained black powders were further immersed in 400 mL 0.5 M H_2SO_4 solution for 24 h at 80 °C and then dried at 60 °C in a vacuum oven for 24 h. These samples are denoted as 'NC-T', where T refers to the pyrolysis temperature (T = 700, 800, 900 °C). For the synthesis of C-900, 1 g MOF-5 was pyrolyzed at 900 °C, washed in 0.5 M H_2SO_4 solution, and dried under vacuum at the same conditions as that of NC-900.

2.4. Electrochemical performance

2.4.1. Preparation of working electrode. For preparation of the electrode, 50 mg catalyst was weighed and suspended in a mixture of tetrahydrofuran (4 mL), Nafion solution (0.5 mL) and

isopropyl alcohol (4 mL). Then the mixture was kept in an ultrasonic bath for 2 h. The suspension was dropcasted onto a carbon cloth electrode with an area of 12.5 cm^2 (2.5 cm × 2.5 cm, both sides effective). The electrode was then dried overnight at 80 °C under vacuum. The final catalyst loading of ~50 mg was confirmed by weighing the working electrode before and after dropcasting process, so the catalyst per area was ~4 mg/cm^2.

2.4.2. CO_2 electrochemical reduction performance. CO_2 electroreduction experiments were performed in a continuous flow reactor as previously reported. The reactor was divided into two compartments, the anode and cathode compartment, by a proton-exchange membrane. The anode compartment contained a counter electrode (Pt gauze), while the cathode electrode contained the working electrode and a reference electrode (Ag/AgCl electrode). Both compartments had a volume of 100 mL, and were filled with 85 mL electrolyte prior to the performance tests, leaving a headspace of 15 mL. CO_2 was then fed into the reactor by bubbling through the liquid with a flow rate of 100 $mL \cdot min^{-1}$ until the electrolyte was saturated, after which the CO_2 flow was fixed at 10 $ml \cdot min^{-1}$. To start the controlled potential electrolysis, an operation potential was applied by a potentiostat (Autolab PGSTAT302N) in the range of -1.0 to -2.0 V vs Ag/AgCl. The cathode compartment was connected to an on-line gas chromatograph (Global Analyzer Solution Compact GC), and the on-line GC would be triggered every 24 min to analyze the gas product. All the experiments last 120 min. At the end of the electrocatalytic test, a liquid sample (~1 mL) was collected from the electrolyte solution for ultra-performance liquid chromatography (UPLC) measurement. After each experiment, the electrochemical reactor was cleaned with distilled water, and the proton-exchange membrane was immersed into 0.1 M H_2SO_4 for regeneration.

Faradaic efficiency (FE) of the gas product was calculated based on the following equation:

$$FE = (n \times F \times v \times f) / (V_m \times j) \quad (1)$$

Where:

n: the number of electrons consumed to produce one product molecule, for the product of CO or H_2 (n=2), while for the product of CH_4 (n=8);

v: the volume fraction of a certain gas product;

f: the overall gas flow rate (in the unit of m^3s^{-1});

F: Faraday constant (F= 96485 $C \cdot mol^{-1}$);

V_m: the molar volume constant at ambient pressure (V_m=0.024465 m^3mol^{-1});

j: steady-state cell current at each applied potential (in the unit of A).

3. RESULTS AND DISCUSSION

3.1. Synthesis and Structural Characterization.

ZIF-8 was synthesized by mixing methanolic solutions of zinc nitrate and MeIm (2-methylimidazole) at room temperature.[44] The powder X-ray diffraction (PXRD) pattern confirms the formation of pure crystalline ZIF-8 (Figure 1a).[46] After pyrolysis and a subsequent acid treatment, the characteristic peaks of ZIF-8 disappear, and two broad reflections positioned at 2θ = 30° and 50.5° are observed in the N-doped carbon samples (Figure 1b), attributed to the (002) and (100) planes of the graphitic carbon, respectively.[40, 47]

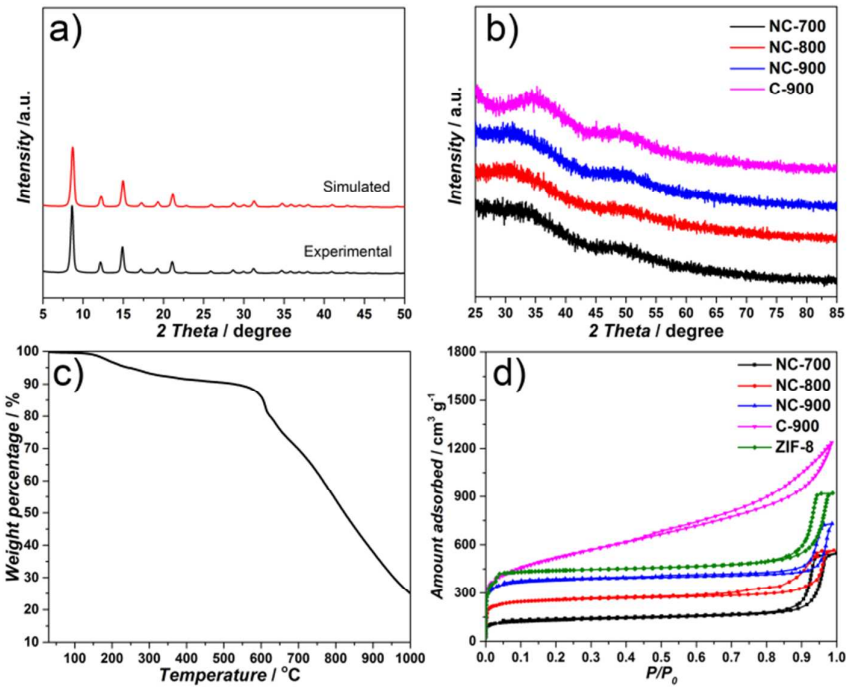

Figure 1. XRD pattern of ZIF-8 (a) and carbon based samples (b); TG curve of ZIF-8 (c); N_2 sorption isotherms of the as-synthesized materials (d).

The graphitization degree of the carbon matrix in the N-doped carbon samples was analyzed by Raman spectroscopy (Figure S1). All the Raman spectra of NC-T exhibit the characteristic G and D bands of carbon at 1580 cm^{-1} and 1350 cm^{-1}, which are correlated to graphitic sp^2 carbon and disordered or defect carbon, respectively.[39] The Raman spectra exhibit an apparent correlation with pyrolysis temperature. The intensity ratio between G and D band (I_G/I_D) is similar between NC-800 and NC-900, suggesting a comparable graphitization degree of the carbon matrix.[48-49] For the Raman spectrum of NC-700, a shoulder at 1500 cm^{-1} can also be observed. This peak is likely to originate from the non-pyrolyzed imidazolates,[50] and leads to an overestimation of the I_G/I_D ratio. Indeed, the presence of non-pyrolyzed imidazolates in NC-700 can be further confirmed by thermogravimetric (TG) analysis (Figure 1c). In the TGA curve, a mass loss of ~ 10 wt.% can be observed until 600 °C, probably attributed to the release of moisture and residual MeIm molecules from the porosity of ZIF-8.[46] The sample mass then decreases sharply with elevating temperature, which can be ascribed to the

decomposition of the organic linker (MeIm) and the gradual evaporation of metallic zinc (boiling point of metallic Zn: 907 °C).[51-52]

The Brunauer-Emmett-Teller (BET) area (S_{BET}) and pore volume (V_{pore}) of ZIF-8 and NC-T samples were determined by N_2 adsorption-desorption isotherms at 77 K (Figure 1d), and the corresponding textural properties are summarized in Table S1. ZIF-8 with a high S_{BET} of 1752 m^2g^{-1} and V_{pore} of 1.42 cm^3g^{-1}, exhibits a typical microporous structure with some intergranular mesoporosity, as concluded from the presence of hysteresis loop above $P/P_0 \approx 0.8$.[53] After pyrolysis and acid leaching, the S_{BET} and V_{pore} of NC-T samples decrease drastically, attributed to the collapse of the well-defined microporous structure of ZIF-8 during the pyrolysis process. Besides, an apparent dependence between surface area and pore volume with pyrolysis temperature can be observed in NC-T samples. Specifically, NC-900 sample exhibits the highest S_{BET} and micropore volume (V_{micro}), but the lowest mesopore volume (V_{meso}) among all NC-T samples, suggesting that a higher pyrolysis temperature can remove more organic residuals from the pores but lead to more agglomeration of carbon nanoparticles.[49]

The morphology of the synthesized materials was studied using electron microscopy. Transmission electron microscopy (TEM) image (Figure 2a) of the as-prepared ZIF-8 exhibits a typical rhombic dodecahedral shape with a size of 30-50 nm. The corresponding energy-dispersive X-ray spectroscopy (EDX) element mapping images (Figure S2a-d) demonstrate the homogeneous dispersion of carbon, nitrogen, and zinc throughout the ZIF-8 crystal. After high-temperature pyrolysis and acid treatment, highly dispersed C, N, and Zn EDX-signals in the pyrolyzed NC-T samples can be detected (Figure S2e-p). The absence of any observable zinc (oxide) nanoparticles in the carbon matrix of the as-synthesized NC-T samples are further verified by TEM analysis (Figure 2b-d), indicating that the acid treatment is sufficient to remove all zinc (oxide) nanoparticles from these nitrogen-doped carbon samples. In

addition, some large pores are observed in the NC-T samples (*e.g.* the yellow circle in Figure 2b), attributed to the presence of voids between nanoparticles, in line with the N_2 sorption results.

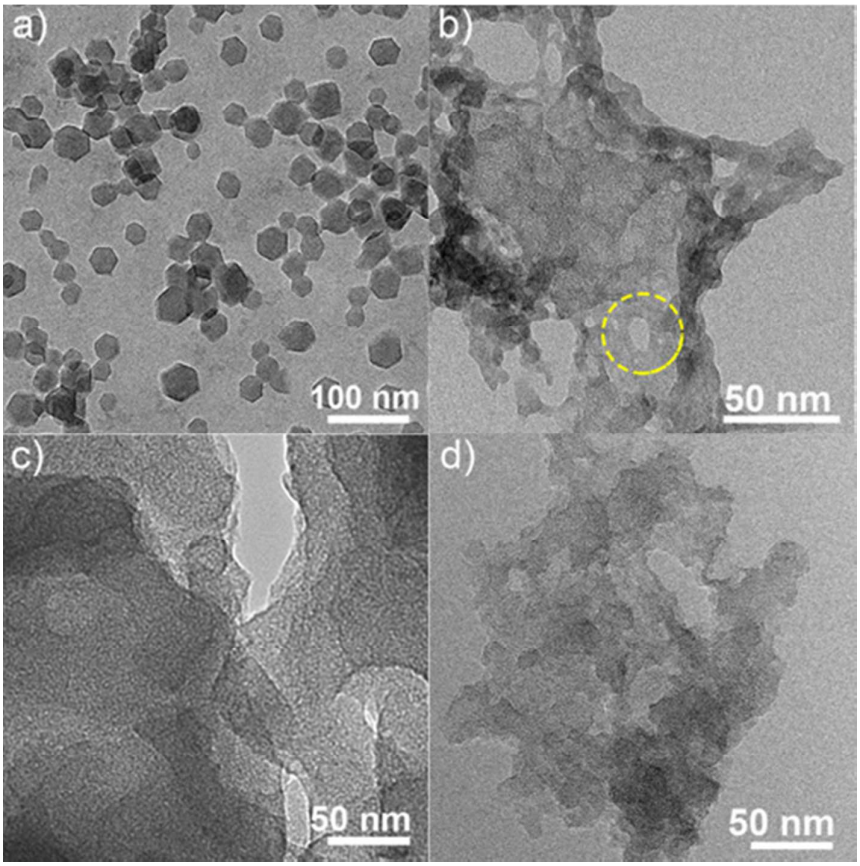

Figure 2. TEM images of ZIF-8 (a), NC-700 (b), NC-800 (c), and NC-900 (d).

The as synthesized precursors and catalysts were further characterized by means of X-ray photoelectron spectroscopy (XPS). The XPS survey spectra clearly demonstrate the presence of C, N, O, and some Zn in the structure of all the samples (Figure S3 a,b and Table S2). XPS survey spectra indicate that these NC-T samples exhibit similar oxygen and zinc contents, and the presence of the O*1s* signal can be attributed to the oxidation of the carbon surface after exposure to the air together with the subsequent acid leaching. The similar Zn contents of NC-T samples detected by XPS analysis further confirm that the acid leaching easily removes those Zn (oxide) nanoparticles in the carbon porosity, while the remaining Zn signals in all

these NC-T samples have been proven by Wang *et al.* to be porphyrin-like Zn ($Zn\text{-}N_x$) with high resistance against acid leaching.[54] N*1s* signals of NC-T samples can be deconvoluted into four types of nitrogen species with binding energy around 398.3 eV, 399.9 eV, 401.2 eV, and 402.5 eV, which can be attributed to pyridinic-N, pyrrolic-N, quaternary-N, and oxidized-N, respectively,[55] as shown in Figure 3a-c. We speculate that, upon pyrolysis, N atoms in the pentagonal ring of the original imidazole units are mostly converted into pyridinic-, pyrrolic-, and quaternary-N species. The percentage of each N species is calculated from XPS analysis and included in Figure 3d and Table S2. Obviously, the NC-T sample synthesized at a higher pyrolysis temperature contains a lower overall N content, which can be attributed to the removal of some relatively unstable N species such as pyridinic and/or pyrrolic-N at high temperature, consistent with previous reports.[55-56] Pyridinic-N dominates in all NC-T samples, and the NC-800 sample has the highest pyridinic-N content of 9.3 %.

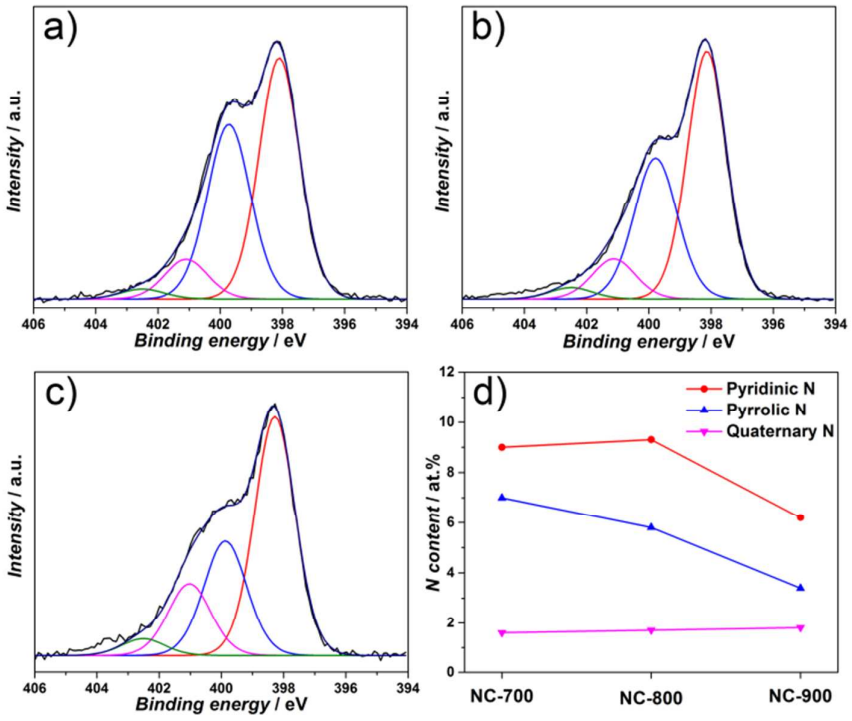

Figure 3. N*1s* XPS region spectra of (a) NC-700, (b) NC-800, and (c) NC-900; (d) N species distribution in NC-900.

3.2. Catalysis

The performance of the N-doped carbon catalysts in the electrocatalytic reduction of carbon dioxide was evaluated in 0.1 M $KHCO_3$ solution saturated with CO_2 under controlled potential electrolysis. No liquid-phase products could be detected during the reaction by ultra-performance-liquid chromatography (UPLC), and the gas products were analyzed by an online gas chromatography (GC). As shown in Figure 4a and b, CO and H_2 are the only detectable reduction products over the whole potential range, except at -1.33 V vs. RHE (reversible hydrogen electrode), where some CH_4 is produced (Figure S4). When the Faradaic efficiency (FE) of CO (FE_{CO}) is plotted as a function of the potential in the range of -0.53 to -1.33 V vs. RHE, a volcano-like curve is obtained, with an optimum at -0.93 V vs. RHE for all these N-doped carbon samples. At the same time, the FE_{CO} of NC-T samples depends on the pyrolysis temperature, and the N-doped carbon pyrolyzed at a higher temperature exhibits a higher FE_{CO}, with NC-900 showing the highest FE_{CO} of ~78% at -0.93 V vs. RHE, which is comparable to the data reported recently from nitrogen-doped carbon catalysts (Table S3).[34-36,57-63] The FE of H_2 (FE_{H2}) exhibits the opposite trend to FE_{CO}, indicating that the electroreduction of CO_2 reaction competes with the hydrogen evolution reaction (HER) in aqueous solutions, which can also be proven by the linear sweep voltammetry (LSV) analysis (Figure S5).[58] Figure 4c and d show the total current density (j_{total}) and partial current density to CO (j_{CO}) for the N-doped carbon samples within the potential range from -0.53 to -1.33 V vs. RHE. NC-900 exhibits the highest j_{total} and j_{CO} among these catalysts. The electrocatalytic stability of the NC-900 sample in CO_2 reduction is as well evaluated by constant potential electrolysis of CO_2 (Figure S6a). At an applied potential of -0.93 V vs. RHE, the NC-900 sample exhibits a stable current density of -1.1 mA cm^{-2} and FE_{CO} of ~80 % during 120 min reaction time, without obvious deactivation.

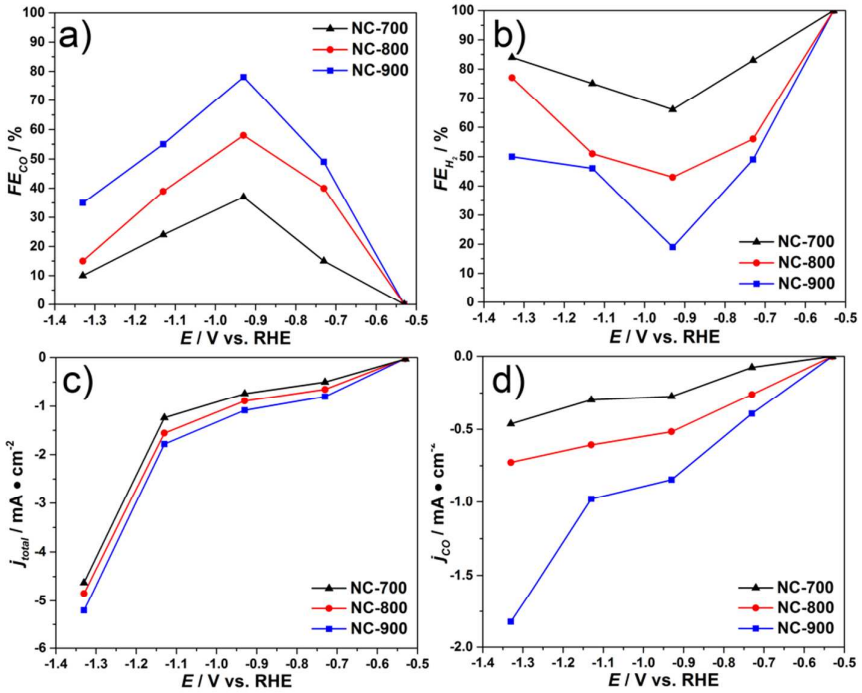

Figure 4. CO_2 electrochemical reduction performance of NC-T samples. (a) Faradaic efficiency to CO, (b) Faradaic efficiency to H_2, (c) Total current density, and (d) Partial CO current density.

To probe the origin of the CO_2 reduction catalytic activity obtained with the NC-900 sample, a carbon material (C-900) was also prepared by pyrolysis of MOF-5 ($[Zn_4O(bdc)_3]$, bdc = benzene-1,4-dicarboxylate),[43] followed by acid leaching under the same conditions as NC-900. As expected, C, O, and Zn signals but no N species can be detected in the XPS survey spectrum of C-900 (Figure S3 and Table S2). Although C-900 exhibits a higher S_{BET} than that of NC-900 (Figure 1d and Table S1), it shows a FE_{CO} as low as ~2%, along with a poor current density of -0.6 mA cm^{-2} at -0.93 V vs. RHE (Figure S6b). This result indicates that the presence of N in the carbon structure significantly improves the activity for CO_2 electroreduction. It has been reported that pyridinic-N and quaternary-N species in the carbon matrix can facilitate the transfer of a proton-electron pair to CO_2, thereby lowering the energy barrier for the production of COOH*, an intermediate for CO formation, resulting in a high catalytic activity, while the pyrrolic-N plays a less important role in this process.[34-35]

Unexpectedly, NC-800 is less active although it has a higher total content of pyridinic-N and quaternary-N than NC-900. On one hand, zinc-porphyrin complex ($Zn\text{-}N_x$) indeed was reported to preferably produce hydrogen under a similar electrochemical measurement condition,[64] however, since NC-900 and NC-800 exhibit similar Zn contents, as proven by XPS analysis, the lower activity of NC-800 cannot be simply attributed to the presence of these Zn species. On the other hand, NC-800 and NC-900 samples also show similar graphitization degrees according to Raman measurement. Thus, we attribute the lower activity of NC-800 mainly to the lower S_{BET} of NC-800, which probably impedes the accessibility of active sites during CO_2 electroreduction process.

4. CONCLUSIONS

We propose a facile route for the preparation of nitrogen-doped carbon materials via pyrolysis of ZIF-8 and a subsequent acid treatment. In CO_2 electroreduction, these N-doped carbon samples are up to 78% selective to CO formation, the higher pyrolysis temperature the better catalytic performance. The high activity can be attributed to the presence of a large amount of pyridinic-N and quaternary-N species in the carbon structure, which are known to lower the energy barrier for the formation of COOH*, an intermediate to produce CO. In addition, the well-developed porosity further promotes the activity by making more active sites accessible.

ASSOCIATED CONTENT

Supporting Information. Figures of catalyst structural characterization, including Raman, SEM-EDX, XPS. Summary of N_2-physisorption and XPS data. Additional CO_2 electroreduction performance. This material is available free of charge via the Internet at http://pubs.acs.org.

AUTHOR INFORMATION

Corresponding Author

* To whom correspondence should be addressed.

E-mail: jorge.gascon@kaust.edu.sa.

Author Contributions

‡R. Wang and X. Sun contributed equally to this work.

Notes

The authors declare no competing financial interest.

ACKNOWLEDGMENT

The authors would like to thank China Scholarship Council (CSC) for the financial support.

REFERENCES

(1) Princiotta, F. T. Global climate change - the technology challenge. *Wit Trans Ecol Envir* **2007,** *101*, 533-551, DOI: 10.2495/Air070531.

(2) Kondratenko, E. V.; Mul, G.; Baltrusaitis, J.; Larrazabal, G. O.; Perez-Ramirez, J. Status and perspectives of CO2 conversion into fuels and chemicals by catalytic, photocatalytic and electrocatalytic processes. *Energ Environ Sci* **2013,** *6* (11), 3112-3135, DOI: 10.1039/c3ee41272e.

(3) Du, G. A.; Lim, S.; Yang, Y. H.; Wang, C.; Pfefferle, L.; Haller, G. L. Methanation of carbon dioxide on Ni-incorporated MCM-41 catalysts: The influence of catalyst pretreatment and study of steady-state reaction. *Journal of Catalysis* **2007,** *249* (2), 370-379.

(4) Park, J. N.; McFarland, E. W. A highly dispersed Pd-Mg/SiO2 catalyst active for methanation of CO2. *Journal of Catalysis* **2009,** *266* (1), 92-97.

(5) Sharma, S.; Hu, Z. P.; Zhang, P.; McFarland, E. W.; Metiu, H. CO2 methanation on Ru-doped ceria. *Journal of Catalysis* **2011,** *278* (2), 297-309.

(6) Shin, H. H.; Lu, L.; Yang, Z.; Kiely, C. J.; McIntosh, S. Cobalt Catalysts Decorated with Platinum Atoms Supported on Barium Zirconate Provide Enhanced Activity and Selectivity for CO2 Methanation. *Acs Catal* **2016,** *6* (5), 2811-2818.

(7) Wang, F.; He, S.; Chen, H.; Wang, B.; Zheng, L.; Wei, M.; Evans, D. G.; Duan, X. Active Site Dependent Reaction Mechanism over Ru/CeO2 Catalyst toward CO2 Methanation. *J Am Chem Soc* **2016,** *138* (19), 6298-6305.

(8) Wang, W.; Wang, S.; Ma, X.; Gong, J. Recent advances in catalytic hydrogenation of carbon dioxide. *Chem Soc Rev* **2011,** *40* (7), 3703-3727.

(9) Bustamante, F.; Enick, R. M.; Cugini, A. V.; Killmeyer, R. P.; Howard, B. H.; Rothenberger, K. S.; Ciocco, M. V.; Morreale, B. D. High-temperature kinetics of the homogeneous reverse water-gas shift reaction. *Aiche Journal* **2004,** *50* (5), 1028-1041.

(10) Daza, Y. A.; Kent, R. A.; Yung, M. M.; Kuhn, J. N. Carbon Dioxide Conversion by Reverse Water-Gas Shift Chemical Looping on Perovskite-Type Oxides. *Ind Eng Chem Res* **2014,** *53* (14), 5828-5837.

(11) Dietz, L.; Piccinin, S.; Maestri, M. Mechanistic Insights into CO2 Activation via Reverse Water–Gas Shift on Metal Surfaces. *The Journal of Physical Chemistry C* **2015,** *119* (9), 4959-4966.

(12) Upadhye, A. A.; Ro, I.; Zeng, X.; Kim, H. J.; Tejedor, I.; Anderson, M. A.; Dumesic, J. A.; Huber, G. W. Plasmon-enhanced reverse water gas shift reaction over oxide supported Au catalysts. *Catalysis Science & Technology* **2015,** *5* (5), 2590-2601.

(13) Wang, L. H.; Liu, H.; Liu, Y.; Chen, Y.; Yang, S. Q. Effect of precipitants on Ni-CeO2 catalysts prepared by a co-precipitation method for the reverse water-gas shift reaction. *Journal of Rare Earths* **2013,** *31* (10), 969-974.

(14) Centi, G.; Perathoner, S. Opportunities and prospects in the chemical recycling of carbon dioxide to fuels. *Catal Today* **2009,** *148* (3-4), 191-205.

(15) Iablokov, V.; Beaumont, S. K.; Alayoglu, S.; Pushkarev, V. V.; Specht, C.; Gao, J.; Alivisatos, A. P.; Kruse, N.; Somorjai, G. A. Size-controlled model Co nanoparticle catalysts for CO(2) hydrogenation: synthesis, characterization, and catalytic reactions. *Nano Lett* **2012,** *12* (6), 3091-3096.

(16) Owen, R. E.; Mattia, D.; Plucinski, P.; Jones, M. D. Kinetics of CO2 Hydrogenation to Hydrocarbons over Iron-Silica Catalysts. *Chemphyschem* **2017,** *18* (22), 3211-3218.

(17) Rungtaweevoranit, B.; Baek, J.; Araujo, J. R.; Archanjo, B. S.; Choi, K. M.; Yaghi, O. M.; Somorjai, G. A. Copper Nanocrystals Encapsulated in Zr-based Metal-Organic Frameworks for Highly Selective CO2 Hydrogenation to Methanol. *Nano Lett* **2016,** *16* (12), 7645-7649.

(18) Saeidi, S.; Amin, N. A. S.; Rahimpour, M. R. Hydrogenation of CO2 to value-added products-A review and potential future developments. *Journal of CO2 Utilization* **2014,** *5*, 66-81.

(19) Satthawong, R.; Koizumi, N.; Song, C.; Prasassarakich, P. Comparative Study on CO2 Hydrogenation to Higher Hydrocarbons over Fe-Based Bimetallic Catalysts. *Top Catal* **2013,** *57* (6-9), 588-594.

(20) Xie, C.; Chen, C.; Yu, Y.; Su, J.; Li, Y.; Somorjai, G. A.; Yang, P. Tandem Catalysis for CO2 Hydrogenation to C2-C4 Hydrocarbons. *Nano Lett* **2017,** *17* (6), 3798-3802.

(21) Ganesh, I. Electrochemical conversion of carbon dioxide into renewable fuel chemicals - The role of nanomaterials and the commercialization. *Renew Sust Energ Rev* **2016,** *59*, 1269-1297.

(22) Lu, Q.; Jiao, F. Electrochemical CO2 reduction: Electrocatalyst, reaction mechanism, and process engineering. *Nano Energy* **2016,** *29*, 439-456.

(23) Pletcher, D. The cathodic reduction of carbon dioxide—What can it realistically achieve? A mini review. *Electrochem Commun* **2015,** *61*, 97-101.

(24) Sastre, F.; Munoz-Batista, M. J.; Kubacka, A.; Fernandez-Garcia, M.; Smith, W. A.; Kapteijn, F.; Makkee, M.; Gascon, J. Efficient Electrochemical Production of Syngas from CO2 and H2O by using a Nanostructured Ag/g-C3N4 Catalyst. *Chemelectrochem* **2016,** *3* (9), 1497-1502.

(25) Whipple, D. T.; Kenis, P. J. A. Prospects of CO2 Utilization via Direct Heterogeneous Electrochemical Reduction. *J Phys Chem Lett* **2010,** *1* (24), 3451-3458.

(26) Zhao, C.; Dai, X.; Yao, T.; Chen, W.; Wang, X.; Wang, J.; Yang, J.; Wei, S.; Wu, Y.; Li, Y. Ionic Exchange of Metal-Organic Frameworks to Access Single Nickel Sites for Efficient Electroreduction of CO2. *J Am Chem Soc* **2017,** *139* (24), 8078-8081.

(27) Thampi, K. R.; Kiwi, J.; Gratzel, M. Methanation and Photo-Methanation of Carbon-Dioxide at Room-Temperature and Atmospheric-Pressure. *Nature* **1987,** *327* (6122), 506-508.

(28) Costentin, C.; Robert, M.; Saveant, J. M. Catalysis of the electrochemical reduction of carbon dioxide. *Chem Soc Rev* **2013,** *42* (6), 2423-2436.

(29) Qiao, J.; Liu, Y.; Hong, F.; Zhang, J. A review of catalysts for the electroreduction of carbon dioxide to produce low-carbon fuels. *Chem Soc Rev* **2014,** *43* (2), 631-675.

(30) Ma, M.; Djanashvili, K.; Smith, W. A. Controllable Hydrocarbon Formation from the Electrochemical Reduction of CO2 over Cu Nanowire Arrays. *Angewandte Chemie* **2016,** *55* (23), 6680-6684.

(31) Back, S.; Kim, J. H.; Kim, Y. T.; Jung, Y. Bifunctional Interface of Au and Cu for Improved CO2 Electroreduction. *ACS Appl Mater Interfaces* **2016,** *8* (35), 23022-23027.

(32) Ma, M.; Trzesniewski, B. J.; Xie, J.; Smith, W. A. Selective and Efficient Reduction of Carbon Dioxide to Carbon Monoxide on Oxide-Derived Nanostructured Silver Electrocatalysts. *Angewandte Chemie* **2016,** *55* (33), 9748-9752.

(33) Liu, Y.; Chen, S.; Quan, X.; Yu, H. Efficient Electrochemical Reduction of Carbon Dioxide to Acetate on Nitrogen-Doped Nanodiamond. *Journal of the American Chemical Society* **2015,** *137* (36), 11631-11636.

(34) Wu, J.; Yadav, R. M.; Liu, M.; Sharma, P. P.; Tiwary, C. S.; Ma, L.; Zou, X.; Zhou, X.-D.; Yakobson, B. I.; Lou, J.; Ajayan, P. M. Achieving Highly Efficient, Selective, and Stable CO2 Reduction on Nitrogen-Doped Carbon Nanotubes. *ACS Nano* **2015,** *9* (5), 5364-5371.

(35) Sharma, P. P.; Wu, J.; Yadav, R. M.; Liu, M.; Wright, C. J.; Tiwary, C. S.; Yakobson, B. I.; Lou, J.; Ajayan, P. M.; Zhou, X.-D. Nitrogen-Doped Carbon Nanotube Arrays for High-Efficiency Electrochemical Reduction of CO2: On the Understanding of Defects, Defect Density, and Selectivity. *Angewandte Chemie International Edition* **2015,** *54* (46), 13701-13705.

(36) Zhang, S.; Kang, P.; Ubnoske, S.; Brennaman, M. K.; Song, N.; House, R. L.; Glass, J. T.; Meyer, T. J. Polyethylenimine-Enhanced Electrocatalytic Reduction of CO2 to Formate at

Nitrogen-Doped Carbon Nanomaterials. *Journal of the American Chemical Society* **2014,** *136* (22), 7845-7848.

(37) Oar-Arteta, L.; Wezendonk, T.; Sun, X. H.; Kapteijn, F.; Gascon, J. Metal organic frameworks as precursors for the manufacture of advanced catalytic materials. *Materials Chemistry Frontiers* **2017,** *1* (9), 1709-1745.

(38) Santos, V. P.; Wezendonk, T. A.; Jaen, J. J.; Dugulan, A. I.; Nasalevich, M. A.; Islam, H. U.; Chojecki, A.; Sartipi, S.; Sun, X.; Hakeem, A. A.; Koeken, A. C.; Ruitenbeek, M.; Davidian, T.; Meima, G. R.; Sankar, G.; Kapteijn, F.; Makkee, M.; Gascon, J. Metal organic framework-mediated synthesis of highly active and stable Fischer-Tropsch catalysts. *Nat Commun* **2015,** *6*, 6451.

(39) Sun, X.; Olivos-Suarez, A. I.; Oar-Arteta, L.; Rozhko, E.; Osadchii, D.; Bavykina, A.; Kapteijn, F.; Gascon, J. Metal-Organic Framework Mediated Cobalt/Nitrogen-Doped Carbon Hybrids as Efficient and Chemoselective Catalysts for the Hydrogenation of Nitroarenes. *Chemcatchem* **2017,** *9* (10), 1854-1862.

(40) Sun, X.; Olivos-Suarez, A. I.; Osadchii, D.; Romero, M. J. V.; Kapteijn, F.; Gascon, J. Single cobalt sites in mesoporous N-doped carbon matrix for selective catalytic hydrogenation of nitroarenes. *Journal of Catalysis* **2018,** *357*, 20-28.

(41) Sun, X.; Suarez, A. I. O.; Meijerink, M.; van Deelen, T.; Ould-Chikh, S.; Zecevic, J.; de Jong, K. P.; Kapteijn, F.; Gascon, J. Manufacture of highly loaded silica-supported cobalt Fischer-Tropsch catalysts from a metal organic framework. *Nat Commun* **2017,** *8* (1), 1680.

(42) Zhang, L.; Su, Z.; Jiang, F.; Yang, L.; Qian, J.; Zhou, Y.; Li, W.; Hong, M. Highly graphitized nitrogen-doped porous carbon nanopolyhedra derived from ZIF-8 nanocrystals as efficient electrocatalysts for oxygen reduction reactions. *Nanoscale* **2014,** *6* (12), 6590-6602.

(43) Liu, B.; Shioyama, H.; Akita, T.; Xu, Q. Metal-organic framework as a template for porous carbon synthesis. *J Am Chem Soc* **2008,** *130* (16), 5390-5391.

(44) Venna, S. R.; Jasinski, J. B.; Carreon, M. A. Structural evolution of zeolitic imidazolate framework-8. *J Am Chem Soc* **2010,** *132* (51), 18030-18033.

(45) Tranchemontagne, D. J.; Hunt, J. R.; Yaghi, O. M. Room temperature synthesis of metal-organic frameworks: MOF-5, MOF-74, MOF-177, MOF-199, and IRMOF-0. *Tetrahedron* **2008,** *64* (36), 8553-8557.

(46) Park, K. S.; Ni, Z.; Cote, A. P.; Choi, J. Y.; Huang, R.; Uribe-Romo, F. J.; Chae, H. K.; O'Keeffe, M.; Yaghi, O. M. Exceptional chemical and thermal stability of zeolitic imidazolate frameworks. *Proceedings of the National Academy of Sciences of the United States of America* **2006,** *103* (27), 10186-10191.

(47) Fei, H.; Dong, J.; Arellano-Jimenez, M. J.; Ye, G.; Dong Kim, N.; Samuel, E. L.; Peng, Z.; Zhu, Z.; Qin, F.; Bao, J.; Yacaman, M. J.; Ajayan, P. M.; Chen, D.; Tour, J. M. Atomic cobalt on nitrogen-doped graphene for hydrogen generation. *Nat Commun* **2015,** *6*, 8668.

(48) Deng, J.; Ren, P.; Deng, D.; Bao, X. Enhanced electron penetration through an ultrathin graphene layer for highly efficient catalysis of the hydrogen evolution reaction. *Angewandte Chemie* **2015,** *54* (7), 2100-2104.

(49) Chaikittisilp, W.; Hu, M.; Wang, H.; Huang, H.-S.; Fujita, T.; Wu, K. C. W.; Chen, L.-C.; Yamauchi, Y.; Ariga, K. Nanoporous carbons through direct carbonization of a zeolitic imidazolate framework for supercapacitor electrodes. *Chemical Communications* **2012,** *48* (58), 7259-7261.

(50) Carter, D. A.; Pemberton, J. E. Raman spectroscopy and vibrational assignments of 1- and 2-methylimidazole. *J Raman Spectrosc* **1997,** *28* (12), 939-946.

(51) Zhong, H. X.; Wang, J.; Zhang, Y. W.; Xu, W. L.; Xing, W.; Xu, D.; Zhang, Y. F.; Zhang, X. B. ZIF-8 derived graphene-based nitrogen-doped porous carbon sheets as highly efficient and durable oxygen reduction electrocatalysts. *Angewandte Chemie* **2014,** *53* (51), 14235-14239.

(52) Torad, N. L.; Hu, M.; Kamachi, Y.; Takai, K.; Imura, M.; Naito, M.; Yamauchi, Y. Facile synthesis of nanoporous carbons with controlled particle sizes by direct carbonization of monodispersed ZIF-8 crystals. *Chem Commun (Camb)* **2013,** *49* (25), 2521-2523.

(53) Xia, B. Y.; Yan, Y.; Li, N.; Wu, H. B.; Lou, X. W.; Wang, X. A metal–organic framework-derived bifunctional oxygen electrocatalyst. *Nat Energy* **2016,** *1*, 15006.

(54) Wang, S.; Shang, L.; Li, L.; Yu, Y.; Chi, C.; Wang, K.; Zhang, J.; Shi, R.; Shen, H.; Waterhouse, G. I.; Liu, S.; Tian, J.; Zhang, T.; Liu, H. Metal-Organic-Framework-Derived Mesoporous Carbon Nanospheres Containing Porphyrin-Like Metal Centers for Conformal Phototherapy. *Adv Mater* **2016,** *28* (38), 8379-8387.

(55) Wu, J.; Liu, M.; Sharma, P. P.; Yadav, R. M.; Ma, L.; Yang, Y.; Zou, X.; Zhou, X. D.; Vajtai, R.; Yakobson, B. I.; Lou, J.; Ajayan, P. M. Incorporation of Nitrogen Defects for Efficient Reduction of CO2 via Two-Electron Pathway on Three-Dimensional Graphene Foam. *Nano Lett* **2016,** *16* (1), 466-470.

(56) Arrigo, R.; Havecker, M.; Schlogl, R.; Su, D. S. Dynamic surface rearrangement and thermal stability of nitrogen functional groups on carbon nanotubes. *Chem Commun (Camb)* **2008,** (40), 4891-4893.

(57) Guo, Y.; Yang, H. J.; Zhou, X.; Liu, K. L.; Zhang, C.; Zhou, Z. Y.; Wang, C.; Lin, W. B. Electrocatalytic reduction of CO2 to CO with 100% faradaic efficiency by using pyrolyzed

zeolitic imidazolate frameworks supported on carbon nanotube networks. *J Mater Chem A* **2017,** *5* (47), 24867-24873.

(58) Wang, H.; Jia, J.; Song, P. F.; Wang, Q.; Li, D. B.; Min, S. X.; Qian, C. X.; Wang, L.; Li, Y. F.; Ma, C.; Wu, T.; Yuan, J. Y.; Antonietti, M.; Ozin, G. A. Efficient Electrocatalytic Reduction of CO2 by Nitrogen-Doped Nanoporous Carbon/Carbon Nanotube Membranes: A Step Towards the Electrochemical CO2 Refinery. *Angew Chem Int Edit* **2017,** *56* (27), 7847-7852.

(59) Xu, J.; Kan, Y.; Huang, R.; Zhang, B.; Wang, B.; Wu, K. H.; Lin, Y.; Sun, X.; Li, Q.; Centi, G.; Su, D. Revealing the Origin of Activity in Nitrogen-Doped Nanocarbons towards Electrocatalytic Reduction of Carbon Dioxide. *ChemSusChem* **2016,** *9* (10), 1085-1089.

(60) Kumar, B.; Asadi, M.; Pisasale, D.; Sinha-Ray, S.; Rosen, B. A.; Haasch, R.; Abiade, J.; Yarin, A. L.; Salehi-Khojin, A. Renewable and metal-free carbon nanofibre catalysts for carbon dioxide reduction. *Nature Communications* **2013,** *4*, 2819.

(61) Lu, X.; Tan, T. H.; Ng, Y. H.; Amal, R. Highly Selective and Stable Reduction of CO2 to CO by a Graphitic Carbon Nitride/Carbon Nanotube Composite Electrocatalyst. *Chemistry* **2016,** *22* (34), 11991-11996.

(62) Jhong, H. M.; Tornow, C. E.; Smid, B.; Gewirth, A. A.; Lyth, S. M.; Kenis, P. J. A Nitrogen-Doped Carbon Catalyst for Electrochemical CO2 Conversion to CO with High Selectivity and Current Density. *ChemSusChem* **2017,** *10* (6), 1094-1099.

(63) Li, W.; Seredych, M.; Rodriguez-Castellon, E.; Bandosz, T. J. Metal-free Nanoporous Carbon as a Catalyst for Electrochemical Reduction of CO2 to CO and CH4. *ChemSusChem* **2016,** *9* (6), 606-616.

(64) Weng, Z.; Jiang, J.; Wu, Y.; Wu, Z.; Guo, X.; Materna, K. L.; Liu, W.; Batista, V. S.; Brudvig, G. W.; Wang, H. Electrochemical CO2 Reduction to Hydrocarbons on a Heterogeneous Molecular Cu Catalyst in Aqueous Solution. *Journal of the American Chemical Society* **2016,** *138* (26), 8076-8079.

Insert Table of Contents artwork here